Heteroatom-Doping Increases Cluster Nuclearity From an [Ag-20] to an [Au3Ag18] Core

Wan-Ting Chang, Sachil Sharma, Jian-Hong Liao, Samia Kahlal, Yu-Chiao Liu, Ming-Hsi Chiang, Jean-Yves Saillard, C. W. Liu

Heteroatom-Doping Increases Cluster Nuclearity: From An $[Ag_{20}]$ to An $[Au_3Ag_{18}]$ Core

Wan-Ting Chang,[a] Sachil Sharma,[a] Jian-Hong Liao,[a] Samia Kahlal,[b] Yu-Chiao Liu,[c] Ming-Hsi, Chiang,[c] Jean-Yves Saillard*[b] and C. W. Liu*[a]

Abstract: A templated galvanic exchange performed on $[Ag_{20}\{Se_2P(OiPr)_2\}_{12}]$ of C_3 symmetry with three equiv. Au^I yields a mixture of $[Au_{1+x}Ag_{20-x}\{Se_2P(OiPr)_2\}_{12}]^+$ (x=0-2) from which $[Au@Ag_{20}\{Se_2P(OiPr)_2\}_{12}]^+$ and $[Au@Au_2Ag_{18}\{Se_2P(OiPr)_2\}_{12}]^+$ are successfully characterized to have T and C_1 symmetry, respectively. Crystal structural analyses combined with DFT calculations on the model compounds explicitly demonstrate that the central Ag^0 of Ag_{20} being oxidized by Au^I migrates to the protecting atomic shell as a new capping Ag^I, and both second and third Au dopants prefer occupying non-adjacent icosahedron vertices. Difference in symmetry, T & C_1, is manifested in the spatial orientation of their protecting atomic shell comprised of 8 capping Ag atoms as well as re-constructing upon the replacement of Ag atoms on the vertices of $AuAg_{12}$ icosahedral core with second and third Au dopants. As a result, a unique pathway for substitutional-doped clusters with increased nuclearity is proposed.

Silver and gold clusters and their alloys[1] in subnanometer range (≤ 2 nm) are currently of keen scientific interests because they exhibit molecule-like properties such as photoluminescence,[2] magnetism,[3] redox behaviour,[4] or chirality[5] not shown by their bulk counterparts. While structurally precise thiolate-[6] and selenolate-protected[7] gold nanoclusters with different metal nuclearities and compositions have been extensively studied, recent advances in nanoscale synthesis also led to the inventions of a few atom-precise thiol- and dithiol-capped homoleptic silver nanoclusters,[8] e.g. $[Ag_{44}(4\text{-FTP})_{30}]^{4+}$,[8a,b] $[Ag_{25}(SPhMe_2)_{18}]^-$,[8c] $[Ag_{20}\{S_2P(OR)_2\}_{12}]$ (R = Pr, *i*Pr),[1e] $[Ag_{21}\{S_2P(OiPr)_2\}_{12}]^+$,[1f] and heteroatom-doped (Au, Pd and Pt) Ag-rich nanoclusters[9] *e.g.* $[Ag_{24}Au(SR)_{18}]^-$,[9a] $[MAg_{24}(SR)_{18}]^{2-}$ (M=Pd/Pt),[9b] $[Pt_1Au_{6.4}Ag_{17.6}(SPhMe_2)_{18}]^{2-}$,[9c] and $[AuAg_{19}\{S_2P(OPr)_2\}_{12}]$.[10] In addition, some mixed thiolate- and phosphine-protected Ag-rich nanoclusters[11] such as $Ag_{29}(BDT)_{12}(TPP)_4$,[11a] $Au_4Ag_{13}(dppm)_3(SR)_9$,[2c] $[PtAg_{28}(BDT)_{12}(PPh_3)_4]^{4-}$,[11b] and $Au_xAg_{50-x}(dppm)_6(SR)_{30}$,[11c] are also known. On the contrary, structurally-precise selenolate-passivated silver nanoclusters are scantily studied. Our group reported the first structurally well-defined silver nanoclusters stabilized by diselenophosphates with compositions $[Ag_{20}\{Se_2P(OiPr)_2\}_{12}]$ and $[Ag_{21}\{Se_2P(OEt)_2\}_{12}]\}^+$, which were prepared by ligand replacement from their S-analogs.[12] We also have been successful in galvanic exchange of the central Ag in the Ag_{13}-centred icosahedron of $[Ag_{21}\{Se_2P(OEt)_2\}_{12}]^+$ by Au while maintaining the same number of metal atoms and a similar molecular structure.[12] All these three structurally precise silver-rich nanoclusters capped by diselenophosphates are found to have 8 superatomic electrons corresponding to the stable $1S^2$ $1P^6$ noble-gas-like electronic configuration.[13] Interestingly, crystal structures of both Ag_{21} and $Au@Ag_{20}$ cores are found to be highly symmetric (T symmetry) compared to that of Ag_{20} (C_3 symmetry). Whereas these three nanoclusters possess similar $Ag@Ag_{12}$ or $Au@Ag_{12}$ centred icosahedral cores, they differ substantially from the arrangement of their protecting shell made of 8 (or 7) capping Ag atoms and 12 diselenophosphate ligands.

So far, all the literature reports on galvanic exchange[9a,10,12]/metal-exchange method[9c,14] of heteroatom doping into homoleptic Ag thiolato nanoclusters result in product clusters with the same number of metal atoms and the shape of metal framework similar to that of the parent cluster. Two such paradigms from the literature are briefly described here. Bakr *et al.* synthesized $Ag_{24}Au(SPhMe_2)_{18}$ via templated galvanic reduction of Au^I by $[Ag_{25}(SPhMe_2)_{18}]^-$.[9a] The trimetallic $[AuPtAg_{23}(SPhMe_2)_{18}]^{2-}$ cluster was synthesized using novel metal-exchange methods[9c,14a] by both Bakr *et al.* and Zhu *et al*. However we have been able to transform $[Au@Ag_{19}\{S_2P(OnPr)_2\}_{12}]$ into a cluster of higher nuclearity with composition $[Au@Ag_{20}\{S_2P(OnPr)_2\}_{12}]^+$ after addition of an Ag^+ ion to the former.[10] Due to the lack of crystal structure of the latter, which prevents detailed understanding of its surface structure, a legitimate mechanistic study in this transformation could not be achieved. It is important to mention here that such a size-structure transformation has still not been examined for heteroatom doping into chalcogenolate-protected silver nanoclusters by structural comparison of both template and target clusters.

Herein we report such a case of galvanic synthesis of $[Au_{1+x}Ag_{20-x}\{Se_2P(OiPr)_2\}_{12}]^+$ (x=0-2) by adding three equiv. Au^+ into $[Ag_{20}\{Se_2P(OiPr)_2\}_{12}]$. Although we got the product clusters with a distribution of compositions (x=0-2), we have been successful in crystallizing $[Au@Ag_{20}\{Se_2P(OiPr)_2\}_{12}]^+$ and $[Au@Au_2Ag_{18}\{Se_2P(OiPr)_2\}_{12}]^+$ from this mixture. The present study reveals a distinct reaction mechanism for substitutional-doped clusters with increased nuclearity. Crystal structural analyses highlight the driving force for building higher nuclearity cluster after the addition of one extra Au atom into the template, $[Ag_{20}\{Se_2P(OiPr)_2\}_{12}]$. Effects of heteroatom doping and differences in symmetry are manifested in significant changes in optical properties as well as on their stability.

The $[Au_{1+x}@Ag_{20-x}\{Se_2P(OiPr)_2\}_{12}]^+$; x=0-2 nanoclusters (NCs) were prepared by galvanic exchange method (see supporting information S1 for details). Briefly, the template $[Ag_{20}\{Se_2P(OiPr)_2\}_{12}]$ cluster and $Au(PPh_3)Cl$ as a source of incoming metal ion, were dissolved in a molar ratio of 1:3 in tetrahydrofuran (5 mL) and the resultant mixture was stirred at 0°C for 2 days under inert atmosphere of N_2. The crude reaction mixture was purified to get pure $[Au_{1+x}Ag_{20-x}\{Se_2P(OiPr)_2\}_{12}]^+$; x=0-2 nanoclusters. The final product was first analyzed by ^{31}P NMR spectroscopy which displays a peak at 64.98 ppm slightly

[a] W.-T. Chang, Dr. S. Sharma, Dr. J.-H. Liao, Prof. C. W. Liu
Department of Chemistry, National Dong Hwa University
No.1, Sec. 2, Da Hsueh Rd. Shoufeng,
Hualien 97401 (Taiwan R.O.C.)
E-mail: chenwei@mail.ndhu.edu.tw
Homepage: http://faculty.ndhu.edu.tw/~cwl/index.htm
[b] Dr. S. Kahlal, Prof. J.-Y. Saillard
Univ Rennes, CNRS, ISCR - UMR 6226, F-35000 Rennes, France
E-mail: jean-yves.saillard@univ-rennes1.fr
[c] Dr. Y.-C. Liu, Dr. M.-H. Chiang
Institute of Chemistry, Academica Sinica
Taipei 115 (Taiwan R.O.C.)
Supporting information and ORCID identification number (s) for the author(s) of this article can be found under:
http://dx.doi.org/xx.xxxx/chem.xxxxxxxxx

downfield-shifted compared to that of 63.9 ppm corresponding to the template cluster $[Ag_{20}\{Se_2P(OiPr)_2\}_{12}]$.[12] The product was further fully characterized using various state-of-the-art techniques such as ESI-Mass spectrometry, X-ray photoelectron spectroscopy, Single crystal X-ray diffraction and UV-Vis spectroscopy.

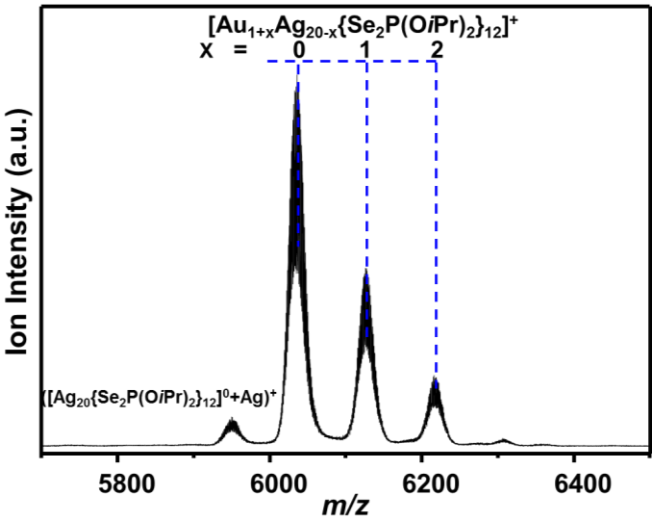

Figure 1. Expansion of positive ion mode ESI-MS of resultant product (mass range *m/z*~5600-6500) after addition of 3 equiv. of Au^+ ion source to the $[Ag_{20}\{Se_2P(OiPr)_2\}_{12}]$ template cluster.

We measured the ESI-MS to find out the chemical composition of resultant clusters after doping Au atoms into template $[Ag_{20}\{Se_2P(OiPr)_2\}_{12}]^0$ clusters. The long-range positive-ion ESI-MS is shown in Figure S1. The spectrum expansion in the range of *m/z*~5600-6500 is shown in Figure 1. It reveals a peak distribution towards higher mass corresponding to compositions $[Au_{1+x}Ag_{20-x}\{(Se_2P(OiPr)_2\}_{12}]^+$; x=0-2. The first and second mass peaks correspond to the compositions $([Ag_{20}\{Se_2P(OiPr)_2\}_{12}]^0+Ag^+)$ (*m/z*~5950) and $[AuAg_{20}\{Se_2P(OiPr)_2\}_{12}]^+$ (*m/z* ~6039), respectively and are thus separated by *m/z*~89. Here a cation Ag^+ assisted in the detection of neutral $[Ag_{20}\{Se_2P(OiPr)_2\}_{12}]$ in ESI-MS. Thus, after the mass correction for cation (Ag^+), the mass difference of *m/z*~197 signifies the addition of one Au atom into the template $[Ag_{20}\{Se_2P(OiPr)_2\}_{12}]^0$ to form $[AuAg_{20}\{Se_2P(OiPr)_2\}_{12}]^+$ without removal of any Ag atom from the former. Here, the change of charged state from 0 to +1 provides the electronic stability ($8e^-$) to the resultant Au doped cluster. Whereas, the mass difference (*m/z*~89) between the second (*m/z*~ 6039), third (*m/z*~6128) and fourth (*m/z*~6217) mass peaks indicates the successive exchange of an Ag atom by an incoming Au atom, starting from $[AuAg_{20}\{Se_2P(OiPr)_2\}_{12}]^+$. The isotopic distributions of the Au doped clusters were found to be in exact match with that obtained by calculations (Figure S2). The peaks in isotopic distributions (Figure S2 A-C) are separated by *m/z*~1 confirms the +1 charge on the resultant clusters. Note that only the first Au atom doping led to an increase of the total number of metal atoms from 20 to 21, whereas subsequent Au-atom doping kept the total number of metal atoms same. Therefore it is reasonable to assume that, unlike the Au doping of $Ag_{25}(SR)_{18}$ reported by Bakr *et al*,[9a] here the Au doping of $[Ag_{20}\{Se_2P(OiPr)_2\}_{12}]$ follows a unique reaction pathway (*vide infra*). To understand this different mechanism of the heteroatom doping and its effect on the properties, it is essential to find out the location of the Au atoms within the skeleton of the $[Au_{1+x}Ag_{20-x}\{Se_2P(OiPr)_2\}_{12}]^+$ (x=0-2) products, through X-ray structure determinations. Crystallization of the chloride salts of $[Au_{1+x}Ag_{20-x}\{Se_2P(OiPr)_2\}_{12}]^+$ were done by vapour diffusion of hexane into a concentrated dichloromethane solution at 10° C. Fortunately, we were successful in crystallizing both $[AuAg_{20}\{Se_2P(OiPr)_2\}_{12}]^+$ (**$AuAg_{20}$**) and $[Au_3Ag_{18}\{Se_2P(OiPr)_2\}_{12}]^+$ (**Au_3Ag_{18}**) chloride salts from the mixture over a couple of weeks.[15]

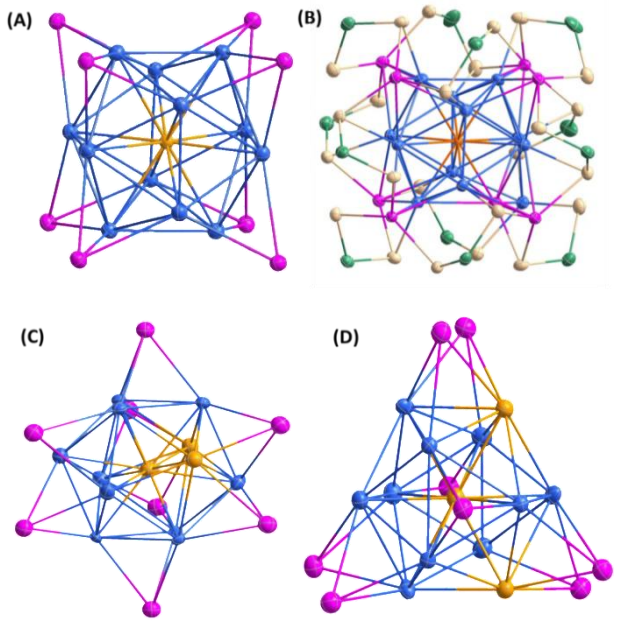

Figure 2. (A) Metal framework and (B) Total structure of $[AuAg_{20}\{Se_2P(OiPr)_2\}_{12}]^+$ super atomic cluster with isopropoxy groups omitted for clarity, (C) A Side view and (D) A top view of metal core in $[Au_3Ag_{18}\{Se_2P(OiPr)_2\}_{12}]^+$. Color legends: blue and purple, Ag; orange, Au; yellow, Se; and green, P.

The metal framework of $[AuAg_{20}\{Se_2P(OiPr)_2\}_{12}]^+$ is shown in Figure 2 (A) and its total structure is shown in Figure 2 (B). It exhibits an $Au@Ag_{12}$ icosahedron engraved in a shell of 8 capping Ag atoms in a cubic arrangement and surrounded by 12 $Se_2P(OiPr)_2$ ligands. The whole cluster is of ideal *T* symmetry and isostructural with the previously reported $[AuAg_{20}\{Se_2P(OEt)_2\}_{12}]^+$ and $[Ag_{21}\{Se_2P(OEt)_2\}_{12}]^+$ clusters.[12] It is worthwhile to mention that this outer shell differs from that of the $[Ag_{20}\{Se_2P(OiPr)_2\}_{12}]$ template, not only by the different number of capping Ag atoms (7), but by their spatial configuration which in the latter case confers to the cluster a structure of ideal C_3 symmetry, which is related to that of $[Ag_{21}\{S_2P(OiPr)_2\}_{12}]^+$.[1f] Furthermore, $[AuAg_{20}\{Se_2P(OiPr)_2\}_{12}](Cl)$ crystallizes in the non-centrosymmetric cubic $P2_13$ space group. However, due to the presence of a racemic mixture in the asymmetric unit shown in Figure S3, the compound is non-chiral as a result.

The chloride salt of $[Au_3Ag_{18}\{Se_2P(OiPr)_2\}_{12}]^+$ crystallizes in the cubic *I*23 space group. The cluster possesses an $Au@[Au_2Ag_{10}]$ centered-icosahedral core (Figure 2 (C) and (D)). Interestingly, both second and third Au atoms prefer occupying non-adjacent icosahedron vertices, rather than outer capping positions. In the crystal, these two Au atoms are randomly distributed in three positions related to the C_3 axis. The disposition of the outer shell (the 8 capping Ag atoms and the 12 ligands) is similar to that in $[Ag_{21}\{S_2P(OiPr)_2\}_{12}]^+$ which is of ideal C_3 symmetry,[1f] as well as that of the $[Ag_{20}\{Se_2P(OiPr)_2\}_{12}]$ precursor (with one less capping atom).[12] As a result, the $[Au_3Ag_{18}\{Se_2P(OiPr)_2\}_{12}]^+$ cation is chiral and of C_1 symmetry.

Various types of M-M and M-Se (M=Au/Ag) bond distances in $[Ag_{20}\{Se_2P(OiPr)_2\}_{12}]$, $AuAg_{20}\{Se_2P(OiPr)_2\}_{12}]^+$, and $[Au_3Ag_{18}\{Se_2P(OiPr)_2\}_{12}]^+$ are evaluated from their crystal structures and are summarized in Table S1. The averaged Au_{center}-Ag_{ico} bond distances in $[AuAg_{20}\{Se_2P(OiPr)_2\}_{12}]^+$, and $[Au_3Ag_{18}\{Se_2P(OiPr)_2\}_{12}]^+$ are calculated to be 2.783(3) Å and 2.779(2) Å, respectively, and are slightly shorter than the averaged Ag_{center}-Ag_{ico} bond distance (2.790(7)Å) in

$[Ag_{20}\{Se_2P(OiPr)_2\}_{12}]$. These are reminiscent of gold being smaller than silver due to relativistic effect. Similarly, the averaged Au_{ico}-Ag_{ico} distance in $[Au_3Ag_{18}\{Se_2P(OiPr)_2\}_{12}]^+$ is observed to be slightly smaller than Ag_{ico}-Ag_{ico} in the template and $[AuAg_{20}\{Se_2P(OiPr)_2\}_{12}]^+$. However, the average Ag_{ico}-Ag_{ico} and Ag_{ico}-Ag_{cap} distances in the template and resultant clusters are found to be of very similar values (Table S1). The spatial orientation of the twelve diselenophosphate ligands around the M_{21} metal framework of $[AuAg_{20}\{Se_2P(OiPr)_2\}_{12}]^+$ and $[Au_3Ag_{18}\{Se_2P(OiPr)_2\}_{12}]^+$ are shown in Figure S4. In both compounds they adopt the same trimetallic-triconnective (μ_2-Se; μ_1-Se) coordination pattern.

In order to rationalize the site preference for the Au atoms in the $[Au_{1+x}@Ag_{20-x}\{Se_2P(OiPr)_2\}_{12}]^+$ (x = 0-2) series, DFT calculations[16] were performed on simplified models in which the $Se_2P(OiPr)_2$ ligands were replaced by Se_2PH_2. Calculations on $[Au@Ag_{20}(Se_2PH_2)_{12}]^+$ starting from the ideal *T* and C_3 configurations of the homometallic species $[Ag_{21}\{Se_2P(OEt)_2\}_{12}]^+$,[12] and $[Ag_{21}\{S_2P(OiPr)_2\}_{12}]^+$,[1f] respectively, found the *T* structure to be the most stable in free energy, in agreement with that of $[AuAg_{20}\{Se_2P(OiPr)_2\}_{12}]^+$ reported above. However, the C_3 structure was found to lie only 1.3 kcal/mol above that of *T* symmetry in free energy. This is consistent with the fact that both architectures correspond to the same electronic description of an 8-electron $[Au@Ag_{12}]^{5+}$ centered icosahedral superatomic core protected by an outer shell composed of 8 Ag^+ and 12 $[Se_2PR_2]^-$ ions. Accordingly, we have earlier shown[12] that in both isomers the Ag natural atomic orbital (NAO) charges are approximately -0.4, +0.2 and +0.6 for the central, surface icosahedral and capping Ag atoms, respectively. The preference of the more electronegative Au for the more electron-rich position yielded the mono-substitution on the central position (with a NAO charge of -0.61) to be favored by 10 kcal/mol and 16-18 kcal/mol over the icosahedral and capping positions, respectively (free energies).

Likewise, we have computed a series of positional $[Au_3Ag_{18}(S_2PH_2)_{12}]^+$ isomers derived from the *T* and C_3 structures described above. Isomers with at least one capping position occupied by Au were found to be disfavoured by at least 10 kcal/mol in total energy. Unsurprisingly, the most stable isomers were found to have the Au atoms occupying the central and two surface icosahedral positions. Among these lower energy structures, which lie in a range of ~ 7 kcal/mol, those in which the two icosahedral Au atoms are not adjacent to each other were found to be slightly privileged. It turns out that the most stable structure (in free energy) was found to correspond to the X-ray structure of $[Au_3Ag_{18}\{Se_2P(OiPr)_2\}_{12}]^+$ described above in Figure 2. Several related isomers found in a range of ~4 kcal/mol above the lowest one are not unlikely to be observed (Figure S5). The closest in energy lies ~2.0 kcal/mol above (free energy). It derives from the *T* structure and has its three Au atoms aligned within the centered icosahedron (Figure S5). In the most stable isomer the computed Au NAO charges are -0.48 (center), -0.10 and -0.11 (icosahedron). That of the icosahedral Ag atoms are in the range +0.22/+0.29 and for the capping Ag there are in the +0.54/+0.58 range.

X-ray photoelectron spectroscopy measurements on $[Au_3Ag_{18}\{Se_2P(OiPr)_2\}_{12}]^+$ are consistent with the structural and DFT results described above. In the survey spectra, peaks attributable to all expected elements were noticed (Figure S6). In Au 4f XPS spectrum (Figure 3 A), the Au $4f_{7/2}$ peak at 83.9 eV suggests the presence of Au as Au^0 (84.0 eV) in the doped cluster. This is consistent with our X-ray and DFT results which indicate that gold atoms belong to the $[Au_3Ag_{10}]^{5+}$ icosahedral core (Figure 2). Further, in the Ag 3d XPS spectrum shown in Figure 3 B, the Ag $3d_{5/2}$ peak can be deconvoluted by curve-fitting process into two peaks attributed to Ag^0 and Ag^I centred at 367.9 and 367.3 eV, respectively. Here Ag^I corresponds to the capping atoms while Ag^0 corresponds to atoms belonging to the $[Au_3Ag_{10}]^{5+}$ core. The atomic ratio (%) of Au to Ag was evaluated to be 14.4/85.6 by XPS, which is in good agreement with expected ratio of Au/Ag (14.3/85.7).

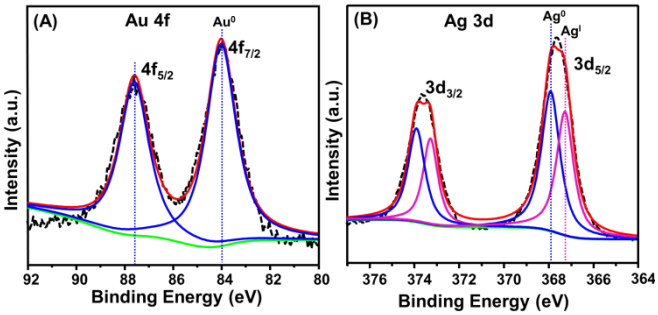

Figure 3. (A) Au 4f XPS spectrum and (B) Ag 3d XPS spectrum of $[Au_3Ag_{18}\{Se_2P(OiPr)_2\}_{12}]^+$ Black dotted line represent the experimental data; red line corresponds to envelop of fitted peaks, Pink and blue lines represent fitted components and green line is base line.

Taking into account the crystal structural and XPS analysis of the doped clusters along with the optimized structures derived from DFT calculations, we propose here a distinct mechanism for doping $[Ag_{20}\{Se_2P(OiPr)_2\}_{12}]$ with Au as depicted in Figure 4.

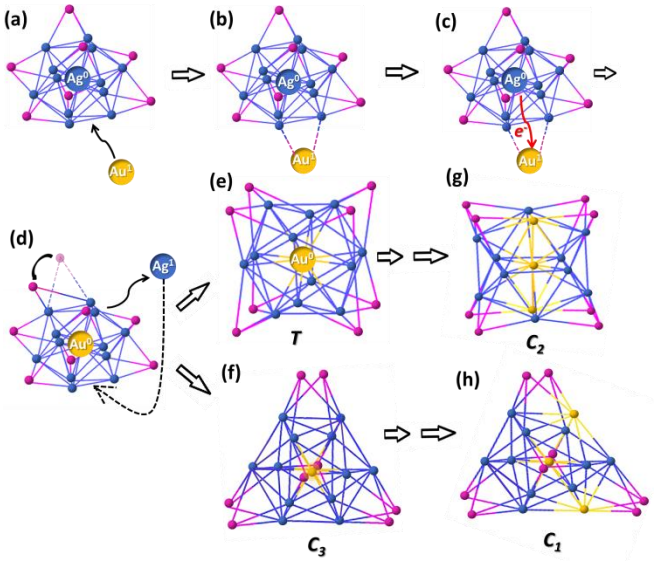

Figure 4. A proposed reaction mechanism of doping of $[Ag_{20}\{Se_2P(OiPr)_2\}_{12}]$ cluster with Au. Color legends: blue, Ag (icosahedral); purple Ag (capping); orange, Au.

The crystal structure of $[Au@Ag_{20}\{Se_2P(OiPr)_2\}_{12}]^+$ suggests that the first Au atom goes to the centre of M_{13} icosahedral core (*vide supra*). This is evidently a one-atom addition reaction, which plausibly occurs via two steps. In the first step (a and b in Figure 4), the addition of Au^I provides the 8th capping atom to form $[(Ag@Ag_{12})(AuAg_7)\{Se_2P(OiPr)_2\}_{12}]^+$. Since gold has a strong preference for the centre of the icosahedral core, the formally Au^I capping atom takes the place of the central Ag^0, the former being reduced in Au^0 and the latter oxidized in Ag^I (i.e. galvanic reduction, as shown in Figure 4c). The expelled Ag^I migrates to a capping position (Figure 4d), thus producing $[(Au@Ag_{12})(Ag_8)\{Se_2P(OiPr)_2\}_{12}]^+$ in *T* or C_3 symmetry (Figures 4e and 4f). Owing to the preference of the subsequent Au dopants for the icosahedral positions and to the stability of the compact M_{21} (M=Ag, Au) cationic structure, further galvanic substitution results in the replacement of a silver atom lying at an icosahedron vertex with an incoming gold atoms (Figures 4g and 4h). Here it is worthwhile to mention that the M_{21} (M = Au, Ag) metal framework of $[Au_{1+x}Ag_{20-x}\{Se_2P(OiPr)_2\}_{12}]^+$ is more symmetrical and hence presumed to be more geometrically stable than the Ag_{20} metal framework of $[Ag_{20}\{Se_2P(OiPr)_2\}_{12}]$, even though both are electronically stable. Hence, the highly

symmetric and relatively more geometrically stable structure of $[M_{21}\{Se_2P(OiPr)_2\}_{12}]^+$; where M=Ag or mixed Au/Ag plays an important role for the reaction pathway described in Figure 4. This is why we consider unlikely the alternative pahtway involving first the formation of an $[Au@Ag_{19}]$ intermediate, subsequently followed by the addition of one Ag^+.

In order to evaluate the effect of gold doping on the cluster optical properties, we investigated the UV-vis absorption features $[Ag_{20}\{Se_2P(OiPr)_2\}_{12}]$ and $[Au_3Ag_{18}\{Se_2P(OiPr)_2\}_{12}]^+$ (Figure 5a). The UV-Vis spectrum of $[Ag_{20}\{Se_2P(OiPr)_2\}_{12}]$ shows two well defined absorption peaks at 498 nm and 418 nm. In $[Au_3Ag_{18}\{Se_2P(OiPr)_2\}_{12}]^+$, the prominent absorption peaks are blue-shifted to 470 nm and 390 nm, respectively. It is noteworthy that in a previous work, very similar types of blue shifts (~28 nm) were also observed when going from $[Ag_{21}\{Se_2P(OEt)_2\}_{12}]^+$ to the gold-centered $[AuAg_{20}\{Se_2P(OEt)_2\}_{12}]^+$.[12]

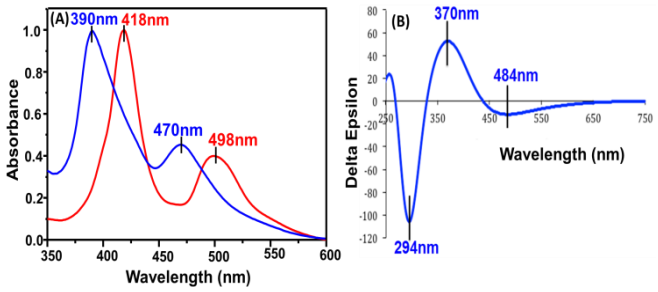

Figure 5. (A) UV-Vis absorption spectra of $[Ag_{20}\{Se_2P(OiPr)_2\}_{12}]$ (red) and $[Au_3Ag_{18}\{Se_2P(OiPr)_2\}_{12}]^+$ (blue) and (B) TD-DFT simulated CD spectrum of $[Au_3Ag_{18}(S_2PH_2)_{12}]^+$.

We further compared the absorption spectra of $[Ag_{21}\{Se_2P(OEt)_2\}_{12}]^+$ and $[Au_3Ag_{18}\{Se_2P(OiPr)_2\}_{12}]^+$ and again similar blue shifts were noticed (Figure S7). Clearly, these data suggest that the presence of an Au atom at the centre of the icosahedron is mainly responsible for perturbation in the UV-Vis absorption spectrum. Other factors such as the molecular charge, the ligand composition or the number of metal atoms (M_{20}/M_{21}) have negligible effects on the electronic structure of the above studied clusters.

In order to test the above hypothesis, time-dependant DFT (TD-DFT) calculations were performed on the $[Ag_{20}(S_2PH_2)_{12}]$ and $[Au_3Ag_{18}(S_2PH_2)_{12}]^+$ models. The corresponding simulated spectra (Figure S8) reproduce qualitatively the above-mentioned blue shift, although the weak low-energy band of $[Au_3Ag_{18}(S_2PH_2)_{12}]^+$ at 543 nm is not experimentally observed. The $[Au_3Ag_{18}(S_2PH_2)_{12}]^+$ peaks at 374, 405, 474 and 543 nm are all associated with transitions involving some of the three highest occupied orbitals (of large central Au character) and some of the six lowest unoccupied orbitals (of large icosahedral Au_2Ag_{10} character). These results fully confirm the role of the central gold atom in the above-mentioned blue-shift. The high-energy peaks at 276 and 302 nm correspond to various MLCT and LMCT transitions. Since the chiroptical responses from the CD spectrum of $[Au_3Ag_{18}\{Se_2P(OiPr)_2\}_{12}]^+$ can not be observed due to the probable isomer-averaging effect on the chiroptical activity,[5] the TD-DFT CD spectrum of an $[Au_3Ag_{18}(S_2PH_2)_{12}]^+$ enantiomer was computed (see Figure 5b). It exhibits three features corresponding to the three major massifs of the absorption spectrum. The intensity of the three extrema on the CD curve is directely related to the involvement of the ligand shell in the corresponding optical transitions. Thus, the CD activity is dominated by the chiral nature of the ligand shell, rather than that of the Au_3Ag_{18} metallic kernel.

The effect of gold doping on the overall stability of the product clusters has been tested under ambient conditions. To this end, time dependent UV-Vis spectra of $[AuAg_{20}\{Se_2P(OiPr)_2\}_{12}]^+$, $[Au_3Ag_{18}\{Se_2P(OiPr)_2\}_{12}]^+$ and $[Ag_{20}\{Se_2P(OiPr)_2\}_{12}]$ clusters were measured at 295 K in acetone (Figures S9 and S10). The $[Ag_{20}\{Se_2P(OiPr)_2\}_{12}]$ cluster in solution was found to be decomposed within 10h. On the contrary, the $[AuAg_{20}\{Se_2P(OEt)_2\}_{12}]^+$,[12] and $[Au_3Ag_{18}\{Se_2P(OiPr)_2\}_{12}]^+$ clusters showed no trace of decomposition till one week. This demonstrates the much higher stability of Au-doped superatomic cationic clusters compared to the neutral $[Ag_{20}\{Se_2P(OiPr)_2\}_{12}]$. The improvement in stability on single Au atom doping of $[Ag_{25}(SR)_{18}]^-$ has also been reported by Bakr *et al*.[9a] The central Au atom doping into the Ag_{13} icosahedron is possibly the key factor in the enhancement of stability of homonuclear Ag-rich nanoclusters.

It is to be noted that the doping of heteroatoms into nanoclusters protected by the same type of ligands usually does not lead to the change of total number of metal atoms in the product cluster. *Substitutional heteroatom doping into homoleptic thiolates- or selenolate-protected Ag nanoclusters yielding a resultant superatom with the different metal nuclearity is not known to the best of our knowledge*. Two notable examples were reported recently by R. Jin *et. al.* in case of Au nanoclusters.[17] Their first report, an heteroatom-induced total structure transformation, is the formation of the heavily Ag-doped $Au_{25-x}Ag_x(SR)_{18;}$ x~19 (R=C_6H_{11}) after reacting $Au_{23}(SR)_{16}^-$ with an Ag(I)-SR complex. In their second report, an heteroatom-induced surface reconstruction, they produced $[Au_{19}Cd_2(SR)_{16}]^-$ (R=C_6H_{11}) via Cd doping into $Au_{23}(SR)_{16}^-$.

In summary, we presented here the first example of diselenolate-protected Ag-rich superatomic alloy, where the Au atom doping into $[Ag_{20}\{Se_2P(OiPr)_2\}_{12}]$ led to $[Au_{1+x}Ag_{20-x}\{Se_2P(OiPr)_2\}_{12}]^+$ (x=0-2) with a metal nuclearity increase from 20 to 21. Based on the crystal structures of $[Ag_{20}\{Se_2P(OiPr)_2\}_{12}]$ $[AuAg_{20}\{Se_2P(OiPr)_2\}_{12}]^+$ and $[Au_3Ag_{18}\{Se_2P(OiPr)_2\}_{12}]^+$ having C_3, T and C_1 symmetries, respectively, along with DFT calculations, we propose a unique reaction pathway not being observed in the substitutional doping of heteroatoms.[17b] The addition of the first dopant atom is followed by galvanic replacement of dopant atoms then re-construction of the outer atomic shell. The increase of metal nuclearity is distinct to previously reported mechanism for Au doping into $Ag_{25}(SR)_{18}$.[9a] We expect that in the future, more efforts will be expanded towards altering the metal nuclearity upon doping the heteroatom into chalcogenolate (thiolate/selenolate) protected Ag nanoclusters.

Acknowledgements

This work was supported by the Ministry of Science and Technology in Taiwan (MOST 106-2113-M-259-010). The GENCI French national computer center is acknowledged for computational resources (grant A0010807367).

Keywords: galvanic replacement • silver • gold • superatom • substitutional doping

[1] a) R. Jin, C. Zeng, M. Zhou, Y. Chen, *Chem. Rev*. **2016**, *116*, 10346-10413; b) H. Qian, M. Zhu, Z. Wu, R. Jin, *Acc. Chem. Res*. **2012**, *45*, 1470-1479; c) R. Jin, S. Zhao, Y. Xing, R. Jin, *CrystEngComm.* **2016**, *18,* 3996-4005; d) W. Kurashige, Y. Niihori, S. Sharma, Y. Negishi, *Coord. Chem. Rev.* **2016**, *320-321*, 238-250; e) R. S. Dhayal, Y.-R. Lin, J.-H. Liao, Y.-J. Chen, Y.-C. Liu, M.-H. Chiang, S. Kahlal, J.-Y. Saillard, C. W. Liu, *Chem. Eur. J*. **2016**, *22*, 9943-9947; f) R. S. Dhayal, J.-H. Liao, Y.-C. Liu, M.-H. Chiang, S. Kahlal, J.-Y. Saillard, C. W. Liu, *Angew. Chem. Int. Ed*. **2015**, *54*, 3702-3706; *Angew. Chem.* **2015**, *127,* 3773-3777; g) W. Kurashige, Y. Niihori, S. Sharma, Y. Negishi, *J. Phys. Chem. Lett.* **2014**, *5*, 4134-4142; h) W. Kurashige, S. Yamazoe, M.

Yamaguchi, K. Nishodo, K. Nobusada, T. Tsukuda, Y. Negishi, *J. Phys. Chem. Lett.* **2014**, *5*, 2072-2076.

[2] a) S. Wang, X. Meng, A. Das, T. Li, Y. Song, T. Cao, X. Zhu, M. Zhu, R. Jin, *Angew. Chem. Int. Ed.* **2014**, *53*, 2376-2380; *Angew. Chem.* **2014**,*126*, 2408-2412; b) G. Soldan, M. A. Aljuhani, M. S. Bootharaju, L. G. AbdulHalim, M. S. Parida, A.-H. Emwas, O. F. Mohammed, O. M. Bakr, *Angew. Chem. Int. Ed*. **2016**, *55*, 5749-5753; *Angew. Chem.* **2016**,*128*, 5843-5847; c) T. Chen, S. Yang, J. Chai, Y. Song, J. Fan, B. Rao, H. Sheng, H. Yu, M. Zhu, *Sci. Adv.* **2017,** *3,* e1700956; d) H. Yu, B. Rao, W. Jiang, S. Yang, M. Zhu, *Coord. Chem. Rev.* **2017,** DOI: 10.1016/j.ccr.2017.12.005.

[3] a) S. Antonello, N. V. Perera, M. Ruzzi, J. A. Gascó n, F. Maran, *J. Am. Chem. Soc* .**2013**,*135,* 15585-15594; b) M. Agrachev, S. Antonello, T. Dainese, M. Ruzzi, A. Zoleo, E. Apra, N. Govind, A. Fortunelli, L. Sementa, F. Maran, *ACS Omega* **2017***, 2,* 2607-2617.

[4] a) A. Dass, S. Theivendran, P. R. Nimmala, C. Kumara, V. R. Jupally, A. Fortunelli, L. Sementa, G. Barcaro, X. Zuo, B. C. Noll, *J. Am. Chem. Soc.* **2015***, 137,* 4610-4613; b) K. Kwak, S. S. Kumar, K. Pyo, D. Lee, *ACS Nano* **2014***, 8,* 671-679; c) J. F. Parker, C. A. Fields-Zinna, R.W. Murray, *Acc. Chem. Res.* **2010**, *43,* 1289-1296.

[5] a) S. Knoppe, T. Bürgi, *Acc. Chem. Res.* **2014***, 47,* 1318-1326; b) I. Dolamic, S. Knoppe, A. Dass, T. Bürgi, *Nature Commun.* **2012***, 3,* 798; c) N. Barrabés, B. Zhang, T. Bürgi, *J. Am. Chem. Soc.* **2014***, 136,* 14361-14364.

[6] a) M. Zhu, C. M. Aikens, F. J. Hollander, G. C. Schartz, R. Jin, *J. Am. Chem. Soc.* **2008**, *130*, 5883-5885; b) H. Qian, W. T. Eckenhoff, Y. Zhu, T. Pintauer, R. Jin, *J. Am. Chem. Soc.* **2010**, *132*, 8280-8281; c) P. D. Jadzinsky, G. Calero, C. J. Ackerson, D. A. Bushnell, R. D. Kornberg, *Science* **2007**, *318*, 430-433; d) Y. Negishi, T. Nakazaki, S. Malola, S. Takano, Y. Niihori, W. Kurashige, S. Yamazoe, T. Tsukuda, H. Hä kkinen. *J. Am. Chem. Soc.* **2015**, *137*, 1206-1212.

[7] a) Y. Song, S. Wang, J. Zhang, X. Kang, S. Chen, P. Li, H. Sheng, M. Zhu, *J. Am. Chem. Soc.* **2014**, *136*, 2963-2965; b) Y. Song, J. Zhong, S. Yang, S. Wang, T. Cao, J. Zhang, P. Li, D. Hu, Y. Pei, M. Zhu, *Nanoscale* **2014**, *6*, 13977-13985; c) Q. Xu, S. Wang, Z. Liu, G. Xu, X. Meng, M. Zhu, *Nanoscale* **2013**, *5*, 1176-1182.

[8] a) A. Desireddy, B. C. Conn, J. Guo, B. Yoon, R. N. Barnett, B. N. Monahan, K. Kirschbaum, W. P. Griffith, R. L. Whetten, U. Landman, T. P. Bigioni, *Nature* **2013**, *501*, 399-402; b) H. Yang, Y. Wang, H. Huang, L. Gell, L. Lehtovaara, S. Malola, H. Hakkinen, N. Zheng, *Nature Commun*. **2013**,4, 2422; c) C.P. Joshi, M. S. Bootharaju, M. J. Alhilaly, O. M. Bakr, *J. Am. Chem. Soc.* **2015**, *137*, 11578-11581.

[9] a) M. S. Bootharaju, C.P. Joshi, M. R. Parida, O. F. Mohammed, O. M. Bakr, *Angew. Chem. Int. Ed*. **2016**, *55*, 922-926; *Angew. Chem.* **2016,** *128*, 934-938; b) J. Yan, H. Su, H. Yang, S. Malola, S. Lin, H. Häkkinen, N. Zheng, *J. Am. Chem. Soc*. **2015**, *137*, 11880-11883; c) X. Kang, L. Xiong, S. Wang, H. Yu, S. Jin, Y. Song, T. Chen, L. Zheng, C. Pan, Y. Pei, M. Zhu, *Chem. Eur. J.* **2016**, *22*, 17145-17150.

[10] Y.-R. Lin, P. V. V. N. Kishore, J.-H. Liao, S. Kahlal, Y.-C. Liu, M.-H. Chiang, J.-Y. Saillard, C. W. Liu, *Nanoscale* **2018**, *10*, 6855-6860.

[11] a) L. G. AbdulHalim, M. S. Bootharaju, Q. Tang, S. D. Gobbo, R.G. AbdulHalim, M. Eddaoudi, D. Jiang, O. M. Bakr, *J. Am. Chem. Soc*. **2015**, *137*, 11970-11975; b) M. S. Bootharaju, S. M. Kozlov, Z. Cao, A. Shkurenko, A. M. El-Zohry, O. F. Mohammed, M. Eddaoudi, O. M. Bakr, L. Cavallo, J.-M. Basset, *Chem. Mater.* **2018**, *30,* 2719-2725; c) W. Du, S. Jin, L. Xiong, M. Chen, J. Zhang, X. Zou, Y. Pei, S. Wang, M. Zhu, *J. Am. Chem. Soc*. **2017**, *139*, 1618-1624.

[12] W.-T. Chang, P.-Y. Lee, J.-H. Liao, K. K. Chakrahari, S. Kahlal, Y.-C. Liu, M.-H. Chiang, J.-Y. Saillard, C. W. Liu, *Angew. Chem. Int. Ed*. **2017**, *56*, 10178-10182; *Angew. Chem.* **2017**,*129,* 10312-10316.

[13] M. Walter, J. Akola, O. Lopez-Acevedo, P. D. Jadzinsky, G. Calero, C. J. Ackerson, R. L. Whetten, H. Gronbeck, H. Hakkinen, *Proc. Natl. Acad. Sci. USA* **2008**, *10,* 9157-9162.

[14] a) M. S. Bootharaju, L. Sinatra, O. M. Bakr, *Nanoscale* **2016**, *8*, 17333-17339; b) X. Kang, S. Chen, S. Jin, Y. Song, Y. Xu, H. Yu, H. Sheng, M. Zhu, *ChemElectroChem* **2016**, *3*, 1-6.

[15] Crystallographic data of $[AuAg_{20}]$: $C_{72}H_{168}Ag_{20}AuClO_{24}P_{12}Se_{24}$, cubic, $P2_13$, $a=b=c=32.8561(14)$ Å, $\alpha=\beta=\gamma=90^o$, $V=35469(5)$ Å^3, $Z=8$, ρ calcd=2.275 g.cm^{-3}, μ=8.067 mm^{-1}, Goodness-of-fit=1.067, $R1$=0.0829, $wR2$=0.2064, 19725 independent reflections [$2\theta \leq 50.00^o$] and 967 parameters. Crystallographic data of $[Au_3Ag_{18}]$: $C_{72}H_{168}Ag_{18}Au_3ClO_{24}P_{12}Se_{24}$, cubic, $I23$, $a=b=c=32.4718(16)$ Å, $\alpha=\beta=\gamma=90^o$, $V=28523.7(11)$ Å^3, $Z=8$, ρ calcd =2.426 g.cm^{-3}, μ=9.840 mm^{-1}, Goodness-of-fit=1.147, $R1$=0.0576, $wR2$=0.1412, 10064 independent reflections [$2\theta \leq 50.00^o$] and 503 parameters. CCDC 1840560 $[AuAg_{20}]$ and 1840561 $[Au_3Ag_{18}]$ contain the supplementary crystallographic data for this paper. These data can be obtained free of charge from The Cambridge Crystallographic Data Centre.

[16] DFT and TD-DFT calculations were carried out at the BP86/Def2-TZVP and CAM-B3LYP/Def2-TZVP level, respectively (see the computational details in the SI).

[17] a) Q. Li, K. J. Lambright, M. G. Taylor, K. Kirschbaum, T.-Y. Luo, J. Zhao, G. Mpourmpakis, S. Mokashi-Punekar, N. L. Rosi, R. Jin, *J. Am. Chem. Soc*. **2017**, *139*, 17779-17782; b) Q. Li, S. Wang, K. Kirschbaum, K. J. Lambright, A, Das, R. Jin, *Chem. Commun*. **2016**, *52*, 5194-5197; c) M. Zhu, P. Wang, N. Yan, X. Chai, L. He, Y. Zhao, N. Xia, C. Yao, J. Li, H. Deng, Y. Zhu, Y. Pei, Z. Wu, *Angew. Chem. Int. Ed*. **2018**, *57*, 4500-4504; Angew. *Chem.* **2018**, *130*, 4590-4594.

A template galvanic replacement reaction of $[Ag_{20}\{Se_2P(OiPr)_2\}_{18}]$ with 3 equiv. Au^{I} yields a 21 metal atom cluster with composition $[Au_{1+x}Ag_{20-x}\{Se_2P(OiPr)_2\}_{12}]^{+}$; x=0-2. Based on crystal structural analysis along with DFT calculations, a distinct reaction pathway was proposed to explain the alteration of metal nuclearity upon Au atom doping. This pathway follows addition, galvanic replacement of dopant, and re-construction of the outer atomic protecting shell.

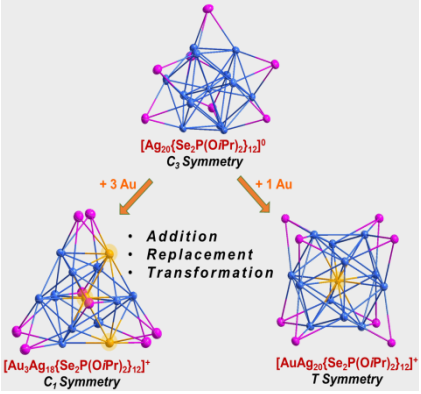

W.-T. Chang, S. Sharma, J.-H. Liao, S. Kahlal, Y.-C. Liu, M.-H. Chiang, J.-Y. Saillard, C. W. Liu**

Page No. – Page No.
Heteroatom-Doping Increases Cluster Nuclearity: From An $[Ag_{20}]$ to An $[Au_3Ag_{18}]$ Core